OPTO-ELECTRONICS REVIEW **14**(1), 19–24

InAs/GaSb superlattice focal plane arrays for high-resolution thermal imaging

R. REHM[1*], M. WALTHER[1], J. SCHMITZ[1], J. FLEIßNER[1], F. FUCHS[1], J. ZIEGLER[2], and W. CABANSKI[2]

[1]Fraunhofer-Institut für Angewandte Festkörperphysik (IAF), Tullastrasse 72, D-79108 Freiburg, Germany
[2]AIM Infrarot-Module GmbH, Theresienstrasse 2, D-74072 Heilbronn, Germany

The first fully operational mid-IR (3–5 μm) 256×256 IR-FPA camera system based on a type-II InAs/GaSb short-period superlattice showing an excellent noise equivalent temperature difference below 10 mK and a very uniform performance has been realized. We report on the development and fabrication of the detector chip, i.e., epitaxy, processing technology and electro-optical characterization of fully integrated InAs/GaSb superlattice focal plane arrays. While the superlattice design employed for the first demonstrator camera yielded a quantum efficiency around 30%, a superlattice structure grown with a thicker active layer and an optimized V/III BEP ratio during growth of the InAs layers exhibits a significant increase in quantum efficiency. Quantitative responsivity measurements reveal a quantum efficiency of about 60% for InAs/GaSb superlattice focal plane arrays after implementing this design improvement.

Keywords: infrared, focal plane array, superlattice, GaSb, thermal imaging.

1. Introduction

Focal plane arrays (FPAs) based on InAs/GaSb short period superlattices (SLs) attract increasing interest for the fabrication of high-performance infrared (IR) imaging systems. As proposed by Smith and Mailhiot [1] in 1987, several groups have shown single detector elements with excellent electro-optical properties, similar to established mercury-cadmium-telluride (HgCdTe) detectors [1–3].

The broken gap type-II band alignment of InAs and GaSb results in an overlap between the GaSb valence band and the InAs conduction band of about 140 meV [4]. For InAs/GaSb SLs with confinement energies exceeding this band overlap, a spatially indirect bandgap opens, which is smaller than the bandgap of its constituents. The effective band gap E_g of these structures can be adjusted from 0.3 eV to values below 0.1 eV by varying the thickness of the InAs layer or by introducing indium in the $Ga_xIn_{1-x}Sb$ layers. InAs/GaSb SLs for mid-IR detection typically consist of InAs and GaSb layers with a thickness between five and fifteen monolayers (ML). Heavy holes are largely confined in the GaSb layers, while electron wave functions overlap considerably from one InAs layer to adjacent InAs layers. The overlap of the electron wave functions results in the formation of an electron miniband in the conduction band. Spatially indirect transitions between the localized holes in the GaSb layers and the electron miniband are employed for the detection of infrared photons in the InAs/ GaSb SL. Due to the localization of holes within the GaSb layers the responsivity in p-i-n superlattice photodiodes is generated by optically excited minority electrons in the intrinsic and p-doped layers, respectively. A scheme of the band structure of an InAs/GaSb SL with an artificial band gap due to carrier confinement of electrons and holes is shown in Fig. 1.

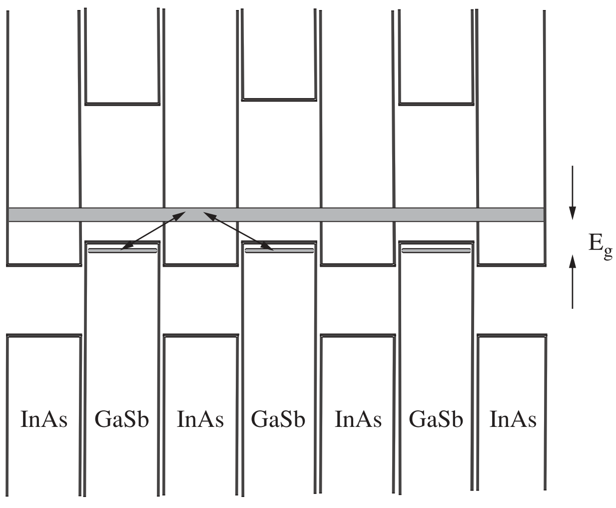

Fig. 1. Schematic band structure of a broken gap type-II InAs/GaSb superlattice. The confinement energy of heavy holes in the GaSb layers is indicated by gray lines, the electron miniband in the conduction band is shown as gray shaded region.

*e-mail: Robert.Rehm@iaf.fhg.de

The paper presented there appears in *Infrared Photoelectronics*, edited by Antoni Rogalski, Eustace L. Dereniak, Fiodor F. Sizov, Proc. SPIE Vol. 5957, 595707 (2005).

The growth of InAs/GaSb short period superlattices is performed by molecular beam epitaxy (MBE). The commercial availability of appropriate substrates constitutes a major advantage. The thickness of the individual layers and the adjustment of the interfaces between adjacent layers in order to control the net strain of the structures is precisely accomplished by MBE.

A major technological challenge for the fabrication of large format FPAs based on InAs/GaSb short-period superlattices with pixel sizes of 40 μm and less is the occurrence of surface leakage currents. Since surface leakage currents in low band gap devices are mostly due to tunneling of electrons, these currents increase exponentially when the band gap of the device shifts to longer wavelengths. Besides efficient suppression of surface leakage currents, a passivation layer suitable for production purposes must withstand various treatments occurring during the subsequent processing and integration up to the camera level. Especially for photodiodes in the 8–12 μm (LWIR) range sufficient reproducibility and long-term stability is difficult to achieve by the deposition of a dielectric passivation layer. Yet a promising method based on the epitaxial overgrowth of LWIR InAs/(GaIn)Sb short-period superlattice mesa devices with lattice matched $Al_xGa_{1-x}As_ySb_{1-y}$ has been demonstrated recently [5]. The present paper focuses on the mid-IR (3-5 μm, MWIR) spectral range where the first fully operational 256×256 SL-camera was demonstrated last year [6].

InAs/GaSb SL-FPAs show a high quantum efficiency and are characterized by an excellent homogeneity of the electro-optical performance combined with very low pixel outages without any large cluster defects. This allows to achieve very low noise equivalent temperature difference (NETD) values at short integration times with InAs/GaSb superlattice FPAs. For the fabrication of staring IR imaging systems based on InAs/GaSb SLs, stable and reproducible growth conditions as well as a reliable processing technology have to be developed.

2. Growth

Samples are grown by MBE in a Gen-II system on undoped (100)-GaSb substrates with 2" diameter. The system is equipped with standard group-III effusion cells for gallium, aluminium and indium and valved cracker cells for arsenic and antimony. Cracker temperatures are held at 800°C for both arsenic and antimony. Silicon and GaTe as well as beryllium can be used for n- and p-type doping.

The detector structure consists of an $Al_{0.5}Ga_{0.5}As_{0.04}Sb_{0.96}$ lattice-matched buffer layer followed by a p-doped GaSb contact layer. Next 190 periods of an InAs/GaSb SL are grown and terminated by a 20 nm thick n-doped InAs cap layer. For mid-IR detector structures the typical thickness for the InAs and GaSb layers is between 5 to 15 ML. The actual composition of the SL region varies depending on the desired cut-off wavelength. The lower part of the SL is p-type doped (1×10^{17} cm^{-3} with Be in the GaSb layers), followed by an undoped region and an n-type doped stack on top of the structure (5×10^{17} cm^{-3} with Si in the InAs layers).

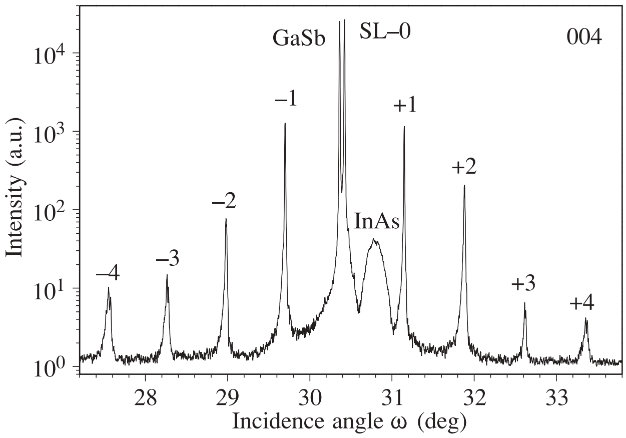

Fig. 2. High resolution x-ray diffraction pattern of the InAs/GaSb detector structure close to the 004 reflection of the GaSb substrate. The diffraction peak of the AlGaAsSb buffer layer is hidden below the substrate peak.

InAs/GaSb SLs on GaSb substrates are under tensile strain due to the smaller lattice parameter of InAs ($\Delta a/a$ = –0.62%). At the transition from GaSb to InAs layers, group III and group V elements are changed. Depending on the shutter sequence during MBE growth, preferential formation of either GaAs or InSb like interface bonds can be forced to introduce an additional source of strain in the layer stack. In particular, InSb like bonds at the interfaces are employed to introduce compressive strain in the InAs/GaSb SL stack to compensate the tensile strain caused by the InAs layers. Details of the strain adjustment and the characterization of InSb or GaAs like interface bonds have been reported elsewhere [7].

Growth conditions, i.e., growth temperature, V/III ratios and shutter sequences have been optimized in order to improve materials quality and to establish a manufacturable growth process. Figure 2 shows the high resolution x-ray diffraction pattern around the 004 reflection of a mid-IR detector structure. The superlattice has a period of 7.06 nm and is under tensile strain with a residual strain of ($\Delta a/a$) = 1.6×10^{-3}. The diffraction pattern reveals well resolved satellite peaks, demonstrating good morphological quality. Formation of InSb like bonds at the InAs/GaSb and the GaSb/InAs interfaces was forced by the shutter sequence during epitaxy in order to match the tensile strain of the InAs. Growth of GaSb was followed by a 1.5 sec antimony soak and the evaporation of 0.5 ML indium without group-V stabilization to form the interface between GaSb and InAs. Switching from InAs to GaSb, 0.5 ML indium was deposited on top of the InAs layer, followed by a 1.5 sec antimony soak for preferential formation of InSb like bonds. Best morphological and optical properties were obtained for a substrate temperature of 390°C, measured with an IR pyrometer. The AlGaAsSb buffer layer and the GaSb contact layer were grown at substrate temperatures of 540°C and 480°C, respectively.

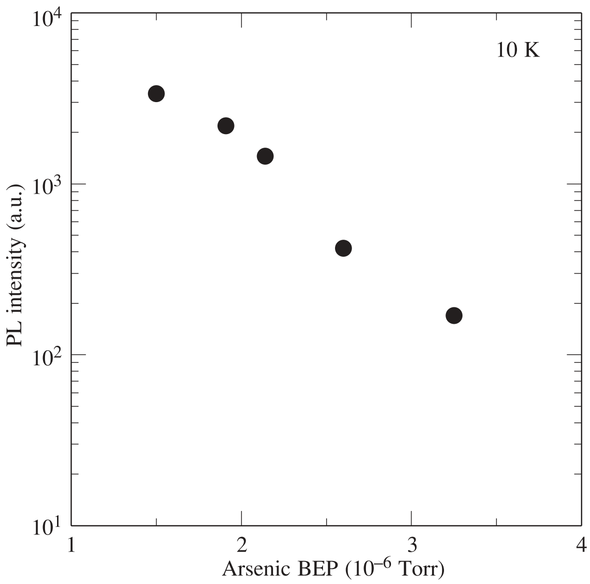

Fig. 3. Photoluminescence yield of an undoped SL emitting at 4 µm wavelength as a function of the arsenic beam equivalent pressure during growth of the InAs layers.

Device properties of the IR-detector depend on the residual doping level and the lifetime of the minority carriers in the superlattice. A strong correlation between PL yield and responsivity was previously observed by our group for long wavelength detectors. PL measurements at 77 K are therefore very helpful to measure bandgap and PL yield of the structures for materials characterization. As an example for PL characterization of InAs/GaSb SLs, the PL yield is plotted as a function of the arsenic beam equivalent pressure during growth of the InAs layers in Fig. 3. PL was measured by Fourier transform infrared spectroscopy at 10 K. It should be noted, that the layer structure used for this investigation consists of an undoped InAs/GaSb superlattice with 190 periods emitting at a wavelength around 4 µm. Growth rates for both GaSb and InAs were set to 1 µm/h and the antimony flux was kept constant at 1.85×10^{-6} Torr for this set of samples, resulting in a V/III beam equivalent pressure (BEP) ratio of 3.4 for GaSb. Reducing the arsenic BEP in the InAs layers from 3.2×10^{-6} Torr (V/III-BEP ratio 5.9) to a value of 1.5×10^{-6} Torr (V/III-BEP ratio 2.7) yields an increase in PL intensity of about a factor of 20. Further reduction of the arsenic flux to 1.2×10^{-6} Torr (V/III-BEP 2.2) however causes a degradation of the surface morphology due to an insufficient supply of arsenic.

3. Process technology

256×256 FPAs with 40 µm pitch are processed as full wafers using standard optical lithography with a mask set which additionally contains various test diodes with different size and geometry. On a single 2” GaSb wafer four FPAs are realized, each with 11.2×11.2 mm^2 area. The process is shown schematically in Fig. 4. Processing starts with the deposition of the ohmic n-contact metalization,

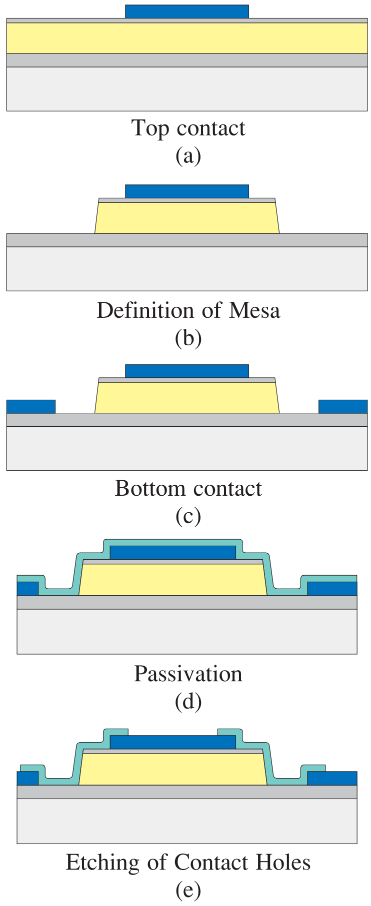

Fig. 4. Processing sequence for the fabrication of 256×256 FPAs on 2”-GaSb.

followed by a dry etching process for mesa definition using Chemically Assisted Ion Beam Etching (CAIBE). Subsequently, the sidewall damage is removed by wet chemical means. After the evaporation of the p-contact metalization, the samples are passivated with a SiO_2-based approach. Subsequently, the dielectric passivation layer on top of the contact metallization is removed by fluorine-based reactive ion etching.

In Fig. 5a, a scanning electron microscope (SEM) image prior to the deposition of the passivation layer is shown. The high selectivity of the wet chemical etchant used for the etch damage removal produces a small step between the GaSb:Be p-type contact layer and the superlattice. Finally, several further metalization layers, which are important for the subsequent hybridization process, are deposited. Figure 5b shows a section of a completely processed 256×256 InAs/GaSb superlattice FPA with 40 µm pitch.

After dicing the wafers, the detector chips are flip-chip bonded onto a read-out integrated circuit (ROIC) using indium solder bump technology. Figure 6 illustrates this process. Following the hybridization with the ROIC, the GaSb substrate is removed by a combination of mechanical lapping, wet-chemical polishing and wet-chemical etching to a thickness of about 20 µm to prevent thermally induced

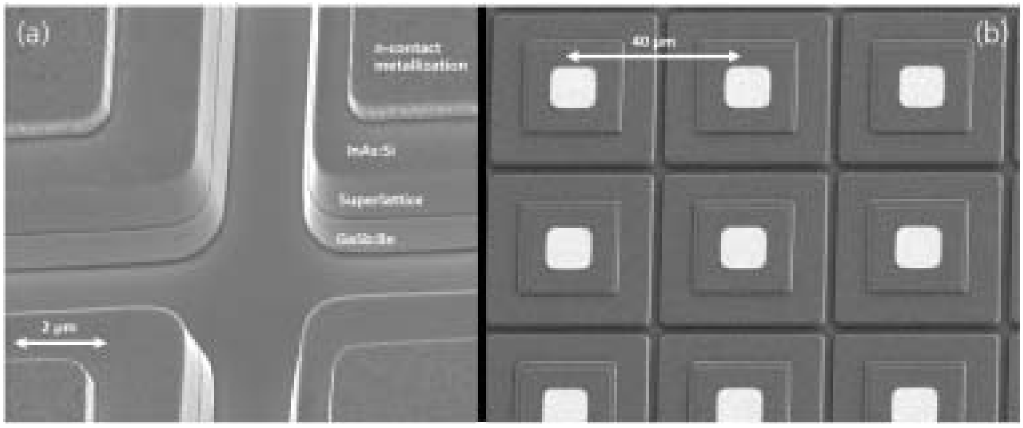

Fig. 5. SEM image of a 256×256 MWIR InAs/GaSb superlattice FPA after CAIBE dry etching of the mesas (a) and at the end of the process prior to hybridization with the silicon readout integrated circuit (b).

stress and to decrease absorption losses due to free carrier absorption in the GaSb substrate. Finally, the detector chip is anti-reflection coated and mounted into an integrated detector cooler assembly with a 1 W linear Stirling cooler.

4. 256×256 mid-IR InAs/GaSb superlattice camera

Based on the technology described above the first 256×256 mid-IR camera was demonstrated last year. The growth sequence of the detector structure started with a 500 nm thick $Al_{0.5}Ga_{0.5}As_{0.04}Sb_{0.96}$ lattice matched buffer layer followed by 700 nm GaSb:Be (3×10^{18} cm^{-3}) representing the p-type contact layer. Subsequently, 190 periods of a 9 ML InAs/10 ML GaSb superlattice were grown. The SL region was terminated by a 20 nm InAs:Si (1×10^{17} cm^{-3}) cap layer acting as an ohmic n-contact layer. For the formation of p-i-n photodiodes the lower 90 periods of the SL were p-doped with 1×10^{17} cm^{-3} Be in the GaSb layers, followed by 40 not intentionally doped periods and 60 periods with a n-type doping of 1×10^{17} cm^{-3} Si in the InAs layers.

Besides the FPA, various test diodes have been fabricated in the full wafer process to characterize the InAs/GaSb SL diodes. The I–V characteristics of diodes in the FPA arrangement can be assessed on test diodes with the same size (37×37 µm^2) and geometry as in the FPA arrangement. At 77 K, dynamic impedance values of R_0A = 4×10^5 Ωcm^2 are obtained at a 5%-cut-off wavelength of

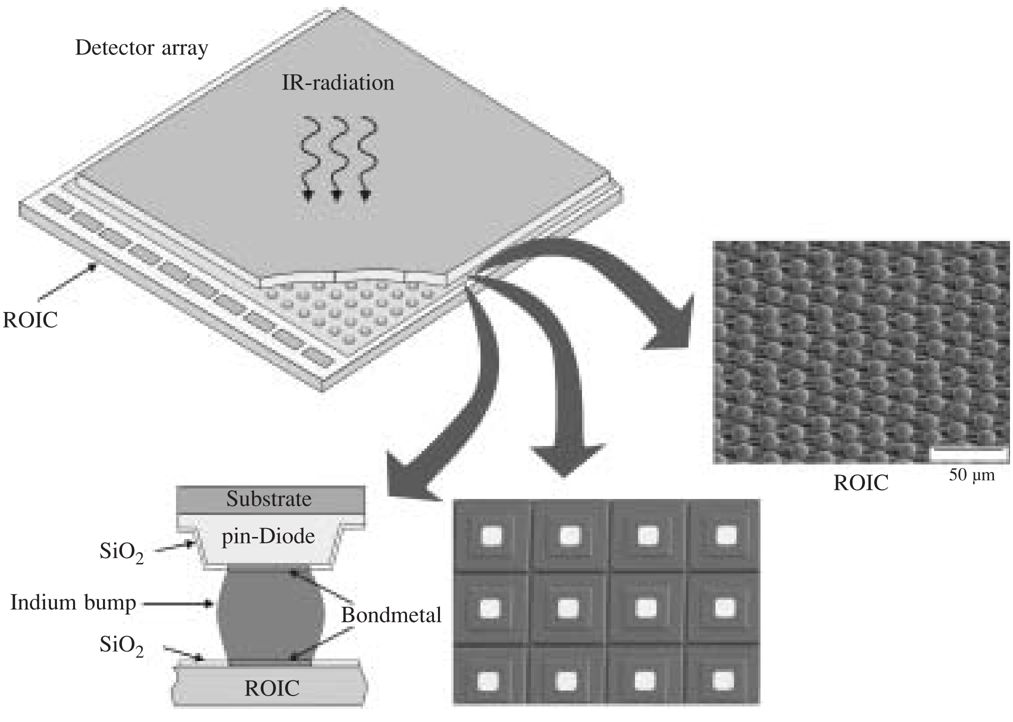

Fig. 6. Scheme of a completely processed 256×256 SL-FPAs, flip-chip bonded to a silicon readout integrated circuit using indium solder bump technology.

5.4 μm. The dynamic impedance increases to values beyond $R_0A = 1\times10^6\ \Omega cm^2$ for a temperature of T = 67 K. The diodes are limited by generation-recombination currents and show background limited performance.

The excellent image quality delivered from the InAs/GaSb SL mid-IR camera system is shown in Fig. 7a. The fine structure of the clothing proves the good spatial resolution and the low cross talk between neighboring detector elements in the FPA.

An important figure of merit is the noise-equivalent temperature difference of the camera system. The distribution of the *NETD* over 256×256 detector pixels at an integration time of 6.5 ms and with F/2 optics is plotted in Fig. 7b. The median *NETD* value is 9.4 mK at a detector temperature of 73 K. For an integration time of 1.25 ms a *NETD* value of 25 mK has been determined. The measured *NETD* values scale inversely proportional to the square root of the integration time between 5 ms and 1 ms, demonstrating background limited performance. The backside-illuminated FPA shows a quantum efficiency around 30% and exhibits very good homogeneity of the *NETD* and excellent spatial uniformity across the entire 256×256 array. Pixel outages are well below 1% and appear statistically distributed, predominantly as single pixel faults without large clusters.

5. Mid-IR photodiodes with high quantum efficiency

Many applications of high performance infrared imagers, e.g., tracking of fast moving objects, require high frame rates and short integration times. Therefore a high conversion rate of incident photons into electrical signal current, i.e. quantum efficiency, is crucial. As discussed in section 2, MBE growth with an optimized arsenic BEP for the InAs layers leads to a significant increase in responsivity presumably due to a decreased recombination rate of minority electrons. Provided that the minority carrier lifetime is sufficiently large, a further improvement of the quantum efficiency should be achievable by increasing the thickness of the p-doped part or the not intentionally doped layer, respectively.

In order to demonstrate this increase of the quantum efficiency samples with thicker active layer were fabricated. Those samples consist of 270 p-doped SL periods with reduced compensation doping of 5×10^{16} cm^{-3} Be in the GaSb layers, followed by 40 not intentionally doped periods and 20 n-doped periods with 5×10^{17} cm^{-3} Si in the InAs layers. For the active region a 9.25 ML InAs/10 ML GaSb SL stack was employed and grown with an optimized arsenic BEP in the InAs layers. The total thickness of the active SL region (without contact layers) is 2150 nm, as compared to 1340 nm in the camera demonstrator and does not cause problems during processing of these structures. Contact and buffer layers are identical in both designs.

The samples were processed according to the description given in section 3. The spectral shape of the responsivity was characterized by standard Fourier transform infrared spectroscopy at 77 K in a cryostat. Lock-in technique with an experimental setup based on a blackbody source combined with a narrow-band IR-filter was used to quantify responsivity values [8]. The IR-filter transmits between 4.6 μm and 5.0 μm with a peak at 4.8 μm resulting in a power density of 11 mW/cm^2. An optical window in the top contact metalization was used for the illumination of the diodes under normal incidence. Therefore, the measured responsivity corresponds to a single optical path of the radiation through the sample. In backside-illuminated FPAs a reflection at the top contact mirror metalization results in double optical path.

(a)

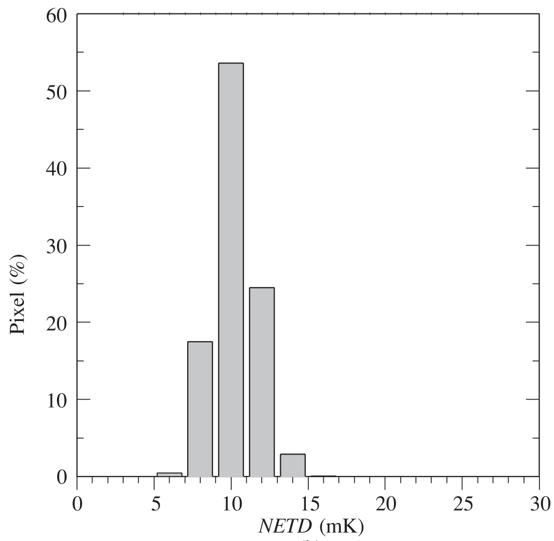

(b)

Fig. 7. Thermal image taken with the 256×256 InAs/GaSb short-period superlattice mid-IR FPA camera system(a). Distribution of the noise equivalent temperature difference (NETD) across the FPA for an integration time of 5 ms and F/2 optics (b).

Considerable effort has been taken in order to determine the transmission coefficient for the incident radiation at the optical diode window. The calculations account for

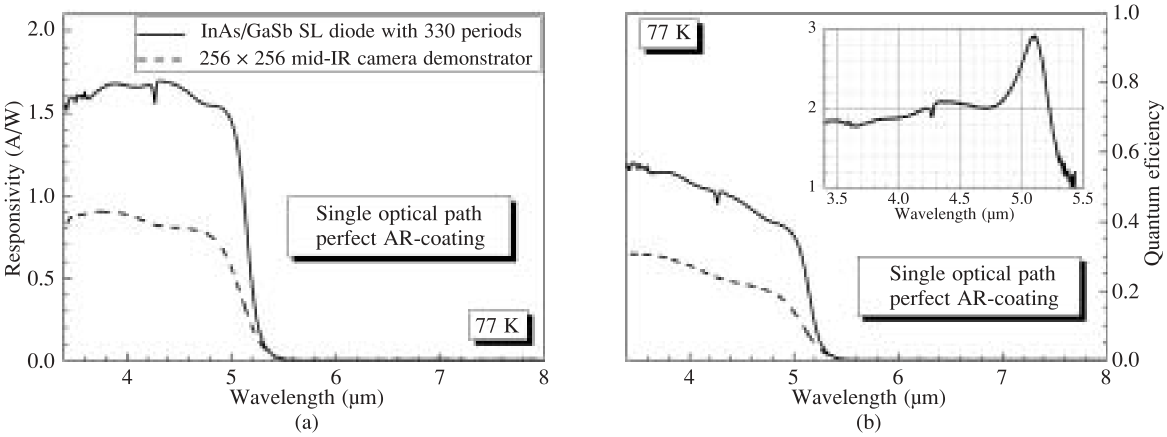

Fig. 8. Comparison of responsivity (a) and quantum efficiency (b) of a InAs/Gab SL photodiode with 330 active periods (solid line) with the 256×256 camera demonstrator comprised of 190 active periods (dashed line). The inset in (b) depicts the quantum efficiency ratio of both structures.

the reflection losses at the interface between vacuum and photodiode including multiple internal interference with attenuation of the reflected beam due to the SL absorption. The results given below correspond to a perfect anti-reflection coating.

Figure 8a compares the responsivity of the 330 period InAs/GaSb SL structure (solid line) with the results obtained on test diodes from the wafer of the 256×256 camera demonstrator described in section 4 (dashed line). The corresponding quantum efficiency is given in figure 8b with an inset depicting the ratio of the quantum efficiency for both samples. The steep increase around the cut-off wavelength for the sample with 330 periods represents an important improvement for camera applications. Samples with 190 periods reveal a responsivity of 0.6 A/W, corresponding to 14% quantum efficiency around 5.0 μm, while samples with 330 periods yield a responsivity of 1.5 A/W and a quantum efficiency of 36%, respectively. Hence, the design with 330 SL periods exhibits roughly 60% quantum efficiency for double optical path in FPA geometry around 5.0 μm.

6. Summary

A 256×256 FPA mid-IR camera system based on InAs/GaSb superlattices with broken gap type-II band alignment has been demonstrated. Detector arrays with a quantum efficiency of 30% and dynamic impedance values of R_0A = 4×10^5 Ωcm^2 at an operation temperature of T = 77 K have been fabricated. Excellent thermal images with low crosstalk between adjacent pixels and *NETD* values below 10 mK are obtained for 5 ms integration time. Further optimization of the MBE growth conditions and an increased thickness of the active layer have led to a significantly improved quantum efficiency of roughly 60% for backside-illuminated FPAs. In conclusion, InAs/GaSb SL are well suited for the fabrication of mid-IR camera systems with a performance level comparable to state of the art HgCdTe detectors.

Acknowledgements

The authors are grateful to K. Schwarz, L. Kirste, H. Güllich and F. Windscheid for characterization of detector structures. We also express out thanks to P. Koidl and G. Weimann for fruitful discussions. Financial support by the German Federal Ministry of Defence is gratefully acknowledged.

References

1. D.H. Chow, R.H. Miles, T.C. Hasenberg, R.A. Kost, Y.H. Zhang, H.L. Dunlap, and L. West, "Mid-wave infrared diode lasers based on GaInSb/InAs and InAs/AlSb superlattices," *Appl. Phys. Lett.* **67**, 3700–3702 (1995).
2. J.L. Johnson, L.A. Samoska, A.C. Gossard, J.L. Merz, M.D. Jack, G.H. Chapman, B.A. Baumgratz, K. Kosai, and S.M. Johnson, "Electrical and optical properties of infrared photodiodes using the InAs/$Ga_{1-x}In_xSb$ superlattice in heterojunctions with GaSb," *J. Appl. Phys.* **80**, 1116–1127 (1996).
3. F. Fuchs, U. Weimer, W. Pletschen, J. Schmitz, E. Ahlswede, M. Walther, J. Wagner, and P. Koidl, "High performance InAs/$Ga_{1-x}In_xSb$ superlattice infrared photodiodes," *Appl. Phys. Lett.* **71**, 3251–3253 (1997).
4. I. Vurgaftman, J.R. Meyer, L.R. Ram-Mohan**, "**Band parameters for III–V compound semiconductors and their alloys," *J. Appl. Phys.* **89**, 5815–5875 (2001).
5. R. Rehm, M. Walther, F. Fuchs, J. Schmitz, and J. Fleissner, "Passivation of InAs/(GaIn)Sb short-period superlattcie photodiodes with 10 m cutoff wavelength by epitaxial overgrowth with $Al_xGa_{1-x}As_ySb_{1-y}$" *Appl. Phys. Lett.* **86**, 173501-1–173501-3 (2005).
6. M. Walther, R. Rehm. F. Fuchs, J. Schmitz, J. Fleißner, W. Cabanski, D. Eich, M. Finck, W. Rode, J. Wendler, R. Wollrab, and J. Ziegler, "256×256 focal plane array midwavelength infrared camera based on InAs/GaSb short-period superlattices, *J. Electron. Mater.* **34**, 722–725 (2005).
7. N. Herres, F. Fuchs, J. Schmitz, K.M. Pavlov, J. Wagner, J.D. Ralston, P. Koidl, C. Gadaleta, and G. Scamarcio, "Effect of interfacial bonding on the structural and vibrational properties of InAs/GaSb superlattices," *Phys. Rev. B* **53**, 15688–15705 (1996).
8. R. Rehm, H. Schneider, K. Schwarz, M. Walther, P. Koidl, and G. Weimann, "Responsivity and gain in InGaAs/GaAs-QWIPs and GaAs/AlGaAs-QWIPs: a comparative study", *Proc. SPIE* **4288**, 379–385 (2001).

